Parametric Investigation of the Effects of Electrical Discharge Machining on Plain D2 Steel

Abual Hassan [1], Ray Tahir Mushtaq [2,*], Aqib Mashood Khan [3,*] and Saqib Anwar [4]

1   Institute of Metal Research, Chinese Academy of Sciences, Shenyang 110016, China; hassan20b@imr.ac.cn or abualhassan666@gmail.com
2   Bio-Additive Manufacturing University-Enterprise Joint Research Center of Shaanxi Province, Department of Industry Engineering, Northwestern Polytechnical University, Xi'an 710072, China
3   College of Mechanical and Electrical Engineering, Nanjing University of Aeronautics and Astronautics, Nanjing 210016, China
4   Industrial Engineering Department, College of Engineering, King Saud University, P.O. Box 800, Riyadh 11421, Saudi Arabia; sanwar@ksu.edu.sa
*   Correspondence: tahirmushtaqray@mail.nwpu.edu.cn (R.T.M.); dr.aqib@nuaa.edu.cn (A.M.K.)

Abstract: Electrical discharge machining (EDM) has emerged as a pivotal non-conventional production technique due to its unique capability to machine without the cutting tool's physical contact with the workpiece, making it apt for brittle, delicate, and complex materials. This research delved into the influence of operational parameters—pulse duration (Ton), peak current (Ip), duty cycle (T), and gap voltage (Vg)—on machining attributes, namely material removal rate (MRR), electrode wear rate (EWR), and radial overcut (ROC) for AISI D2 steel. Utilizing the Taguchi L9 orthogonal array for experimental design, nine experiments were conducted, followed by signal-to-noise ratio (S/N ratio) computations. Key findings highlighted a 4.02 dB improvement in the S/N ratio for MRR, leading to a 29.13% improvement; a 10.35 dB enhancement in the S/N ratio for EWR, resulting in a 33.33% reduction; and a 2.20 dB increase in the S/N ratio for ROC, leading to a 28.57% increment. ANOVA analyses further underscored the predominant influence of all four parameters. The significance of these findings lies in optimizing the EDM process for increased efficiency, reduced tool wear, and enhanced precision, potentially leading to cost savings and improved production quality in industrial applications.

Keywords: electrical discharge machining; dielectric medium; non-conventional machining; process parameters; material removal rate

1. Introduction

Many conventional techniques of cutting cannot be employed as they would damage the expensive material [1]. Electrical discharge machining (EDM), also called the non-conventional machining process, harnesses electrical energy to produce sparks that erode material [2,3]. In this process, the tool approaches the material, establishing a specific gap. This gap is crucial for the ionization of the dielectric with the desired voltage [4]. The absence of direct tool-to-workpiece contact ensures there are no mechanical stress, chatter, or vibration problems during machining [5,6]. EDM's erosion mechanism primarily capitalizes on converting electrical energy into thermal energy, utilizing the dielectric liquid medium [7,8]. The plasma channel, formed between the cathode and anode, becomes heated to temperatures between 8000 and 12,000 °C. This process involves voltage pulses that lead to the dielectric fluid's electrical breakdown, necessitating high-voltage current for discharge [9–11].

The essential components of EDM include EDM circuits, a dielectric unit, and a servo feed control system [12]. Each of these components plays a crucial role in ensuring the efficiency and precision of the EDM process [13]. Several parameters influence the

EDM process, including pulse duration, pulse interval, electrode gap, duty cycle, and polarity [14,15]. These parameters, particularly electrical ones like pulse duration and interval, are integral to achieving optimal machining results [16–18]. Primarily, there are two types: die-sinking EDM and wire EDM [19]. Both serve specific purposes and have unique advantages suited to varied manufacturing needs [20,21].

EDM's advantages range from crafting complex shapes [22] and machining tough materials [23] to ensuring high precision [24]. However, it is not without drawbacks, including slow material removal rates and high power consumption. EDM's applications span various industries, from aerospace to automotive R&D [25,26]. Its ability to machine hard materials and deliver precision makes it a staple in modern manufacturing [27–29]. With the growing demands of precision, efficiency, and versatility in the manufacturing world, understanding and optimizing EDM's parameters becomes paramount [30]. This project aims to delve into this aspect, seeking optimal parameters for machining D2 steel with EDM.

EDM has gained significant attention in recent years. Researchers globally have endeavored to enhance and understand its process parameters [31,32]. This literature review collates such findings, offering insights into the diverse parameters affecting EDM's output and efficiency. Several studies highlight the importance of process parameters in influencing the outcome of the EDM process [33–35], particularly in terms of material removal rate (MRR), electrode wear rate (EWR), and rate of cut (ROC).

The inspection of MRR, roughness of the surface overcut, along with clearance, was performed by change of input factors such as voltage, current values, time (pulse on), and electrode distance [36]. The performance parameters of the Ti-6Al-4V alloy were measured utilizing a maglev EDM operation with bio-dielectrics made of canola and neem oils. Comparing the outcomes for each bio-dielectric at different discharge voltages (22, 25, and 28 V) while varying the discharge current (220–250 mA) was performed. In comparison to EDM oil, the performance assessment shows (25–28) lower SE consumption in neem oil and (35–37) in canola oil. Using bio-dielectrics, the examination of surface morphology shows reduced deformities and improved homogeneity [37]. According to research, composite coatings over the electrode have lower weldability and a lower tool wear rate than other metals. They also increase conductivity and can be flushed and correctly sliced. [38]. Research shows that using certain additives in the dielectric that combine with the dielectric improves dimensional accuracy, minimizes tool wear rates, and boosts the surface smoothness of the machined specimen [39].

This research holds immense relevance as EDM becomes increasingly integral in industries, especially when dealing with materials like D2 steel [40]. In this study, the authors investigated the effects of key EDM parameters on D2 steel machining characteristics. The parameters include pulse duration (ranging from 80 µs to 160 µs), peak current (from 10 A to 18 A), duty cycle (7% to 13%), and gap voltage (55 V to 65 V). These parameters were chosen based on their significant impact on outcomes like the material removal rate, electrode wear rate, and radial overcut, providing insights into the optimal conditions for the EDM machining of D2 steel.

The insights gained will be invaluable for industries aiming for economic efficiency, better production rates, and time conservation [41–43]. While much has been studied about EDM, there remains a gap in understanding the optimal parameters for machining specific materials like D2 steel. This project aims to fill this gap, striving to pinpoint parameters that maximize efficiency and precision, thereby benefitting industries extensively using EDM.

2. Materials and Methods

2.1. Materials

The investigation employed D2 steel measuring 90 × 70 mm with a depth of 10 mm. D2 AISI is a high-carbon, high-chromium metal crafted for functions necessitating superior wear or abrasion resistance and resilience to significant pressure rather

than abrupt impacts. Due to these attributes and its stability against deformation, D2 AISI stands unparalleled for die tasks in extended production sequences. Predominantly, it is an oil-hardening material, and it solidifies profoundly. D2 AISI metal is also recognized as 1.2379 and is an air-hardening, high-carbon, high-chromium instrument metal. It showcases exceptional resistance to wear and possesses favorable dimensional consistency and elevated compressive robustness. It achieves a hardness spectrum of 58–62 HRC [44]. Given its resistance to abrasion in the solidified state, the machining of D2 AISI tends to focus on surface refinement. Its mass is approximately 7700 kg/m^3. The constituents of AISI D2 steel are delineated in Table 1.

Table 1. The composition of AISI D2 Steel.

Elements	Weight (%)
Carbon	1.4–1.6
Chromium	11–12
Molybdenum	0.70–1.20
Manganese	0.6
Silicon	0.6
Phosphorus	0.030
Sulfur	0.030

The corrosion coating was eliminated through grinding to enhance the conductivity of the D2 AISI steel sheet. Mechanical attributes refer to those characteristics that demonstrate the flexible or inflexible response of a substance when exposed to forces encompassing bending, fragility, stretching, rigidity, and tensile robustness. Other attributes related to thermal or procedural aspects are elaborated upon in Table 2.

Table 2. Mechanical, thermal, and processing properties of AISI D2 steel and copper tool electrodes are mentioned.

Properties	Values
Rockwell Hardness, C (AISI D2 Steel)	58–62 HRC
Strength (AISI D2 Steel)	600–700 MPa
Yield Strength (AISI D2 Steel)	400 MPa
Elastic Modulus (AISI D2 Steel)	190–210 GPa
Specific Gravity (AISI D2 Steel)	7.87
Density (AISI D2 Steel)	7700 kg/m^3
Electrical Resistivity (AISI D2 Steel)	54.8 μOhm-cm at 21 °C
Elongation at Break (AISI D2 Steel)	4–10%
Poisson Ratio (AISI D2 Steel)	0.27–0.30
Machinability (AISI D2 Steel)	Fair to Poor
Melting Point (AISI D2 Steel)	1510 °C
Forging (AISI D2 Steel)	1050 °C–900 °C
Annealing (AISI D2 Steel)	850 °C
Rockwell Hardness, B (Copper tool)	45 HRB
Tensile Strength (Copper tool)	210–345 MPa
Yield Strength (Copper tool)	115–125 MPa
Elastic Modulus (Copper tool)	117 GPa
Specific Gravity (Copper tool)	8.96
Electrical Resistivity (Copper tool)	1.70×10^6 Ω cm at 20 °C
Elongation at Break (Copper tool)	40%
Poisson Ratio (Copper tool)	0.20–0.30
Machinability (Copper tool)	Excellent
Heat of Fusion (Copper tool)	204.8 J/g
Heat of Vaporization (Copper tool)	5234 J/g
Specific Heat Capacity (Copper tool)	0.385 J/g-°C

A round copper (Cu) electrode, measuring 9.60 mm in diameter, was used for EDM, as depicted in Figure 1. Copper is a remarkable electrical conductor, possessing minimal electrical resistance approximated at 1.70×10^6 Ω cm. This limited resistance denotes that electricity can flow through Cu efficiently at a significant pace. Copper also boasts notable corrosion resistance, non-magnetic properties, pronounced metallic sheen, elevated ductility, and also functions as a potent antimicrobial agent. Comprehensive specifications about Cu's mechanical and thermal attributes are also presented above in Table 2.

Figure 1. Tool electrode used in machining.

2.2. Methods

Design of Experiments and Research Methodology

Machining tests were conducted utilizing a CNC die-sinking EDM (17U4558) (AgieCharmilles, Geneva, Switzerland) with kerosene oil serving as the dielectric. Both electrodes (the tool and the workpiece) were submerged in a kerosene environment under reverse polarity configuration, with the intricate machining arrangement. The choice of kerosene as the dielectric fluid in this study, despite mineral oil being more promising from a technological and environmental standpoint, was driven by a specific research interest. Kerosene, being less expensive than mineral oil, is widely used in various industrial settings. Our study aims to analyze the interaction of AISI D2 steel and copper electrodes in the context of kerosene as the dielectric medium, which has not been extensively studied before. This approach provides a unique perspective on the EDM process using a more cost-effective medium, contributing to the body of knowledge in EDM research. The EDM machines used in this research are shown in Figure 2.

Figure 2. EDM machine used in research.

While the comprehensive factorial design offers an in-depth comprehension of the implications of processing, it demands significant financial and temporal resources. In contrast, Taguchi's fractional factorial design facilitates a detailed evaluation, optimizing time by curtailing the number of tests yet sustaining a commendable precision [45]. Consequently, the Taguchi fractional factorial design (L9 orthogonal array) was chosen for the planning of the machining trials, delineated in Table 3. Prior to conclusive experimentation, preliminary tests and an exhaustive review of the literature were undertaken to discern the levels of parameters and their respective influences on machining.

Table 3. Experiments and their results with D2 Steel.

Ip (A)	Vg (V)	Ton (μs)	T (%)	MRR (g/min)	EWR (g/min)	ROC (mm)
10	55	80	7	0.0713	0.00228	0.212
10	60	120	10	0.0927	0.00494	0.2042
10	65	160	13	0.10039	0.006471	0.2204
14	55	120	13	0.089356	0.001544	0.2183
14	60	160	7	0.05306	0.0035294	0.223
14	65	80	10	0.113906	0.00634	0.2567
18	55	160	10	0.0642	0.0003718	0.2292
18	60	80	13	0.112	0.0032158	0.25
18	65	120	7	0.089022	0.0055	0.285

The machining setup consists of fundamental visual representations pertaining to die-sinking electrical discharge machining (EDM), the workpiece, and the tool electrode. The study incorporated various process characteristics, including pulse on time (Ton) measured in seconds, peak current (Ip) measured in amperes, duty cycle (T) without any unit, and gap voltage (Vg) measured in volts, whereas the output responses were comprised of radial overcut (ROC, mm), electrode wear rate (EWR, mm^3/min), and material removal rate (MRR, mm^3/min).

The MRR and EWR computations were conducted by gathering machining data pertaining to cycle duration, workpiece mass, and tool electrode measurements prior to and following each machining cycle. The radial overcut was measured using the Chen Wei GS-121510, a three-axis coordinate measuring machine (CMM) (THOME Präzision GmbH, Messel, Germany). The equations for measuring ROC, EWR, and MRR have been mentioned.

$$\text{ROC} = \frac{(D_h - D_e)}{2} \tag{1}$$

$$\text{EWR} = \frac{V_e}{T} \tag{2}$$

$$\text{MRR} = \frac{V_h}{T} \tag{3}$$

The symbols D_h and D_e are used to represent the diameters of the machined hole and tool electrode, respectively. The variable V_e denotes the volume of the eroded electrode in grams, while V_h represents the volume of the drilled hole in the workpiece in grams. And mb and ma are used to denote the mass of the work material before and after the complete machining cycle, respectively. Lastly, T represents the duration of the machining cycle required for each experimental run. The weight of the workpiece and tool electrode was determined using a Denver instrument T-214 (Antylia, Shanghai, China), which is a highly exact electronic scale. The occurrence of spark erosion in AISI D2 steel is visually depicted in Figure 3, providing a physical representation of this process [46,47].

Figure 3. The phenomenon of spark erosion in AISI D2 Steel.

3. Results and Discussion

3.1. Taguchi Procedure

The deviation function utilized by Genichi Taguchi [48] denotes the difference between actual and target values in terms of the signal-to-noise metric. This proportion of averages to variability is represented by the S/N indicator. This study indicates that improving surface integrity is achieved by reducing MRR, EWR, and ROC [49]. The results and trials are showcased in Table 3. Minitab 21.3 served as the tool for performing the Taguchi evaluation. To enhance the precision of our experiment, we employed the Taguchi L9 orthogonal array for experimental design. This method effectively balances the intricacy of a comprehensive factorial design with the practical constraints of time and resources. By selecting key parameters like pulse duration, peak current, duty cycle, and gap voltage, we were able to systematically evaluate their impact on crucial machining attributes such as MRR, EWR, and ROC.

3.2. Effects of the EDM Parameters on MRR

Electrical discharge machining (EDM) is a well-recognized machining technique known for its capability to shape hard metals and alloys which are electrically conductive. The efficiency of the EDM process largely hinges on the optimization of its operating parameters. In the context of the present study, the primary EDM parameters explored include Ip (Amp), Vg (volt), Ton (μs), and T.

For instance, in the EDM process, the parameter Ip (Amp) denotes the current pulse, which is vital for discharging energy. An inadequate current pulse would not provide sufficient energy for material removal [50], while an excessive pulse might lead to unnecessary energy consumption and potential damage to the workpiece. Therefore, based on initial testing, the parameter values for Ip were determined to be set within a feasible and efficient range.

The results demonstrate that there are notable variations in MRR when different EDM parameters are manipulated. To be precise:

- Varying the Ip (Amp) led to a change in MRR. The delta value associated with Ip was found to be 0.00297, placing it at rank 4 in terms of its significance on the MRR.
- Altering the Vg (volt) demonstrated a clear impact on the MRR. With a delta value of 0.02615, Vg ranks third in terms of its influence on MRR.
- Ton (μs), the on-time duration of the pulse, was also instrumental. Its change led to a delta value of 0.02652, making it the second most significant parameter affecting MRR.
- The parameter T emerged as the most critical, with the highest delta value of 0.02945, ranking it first in significance.

These findings emphasize the paramount importance of the parameter T in the EDM process, with other parameters like Vg and Ton also playing significant roles [51]. In contrast, Ip has the least influence on MRR among the considered parameters [52–54].

The chosen parametric values were derived from thorough preliminary experiments to ascertain optimal settings for the EDM process. Lower or higher values were initially considered; however, they were either found inefficient or posed potential risks to the machining process. The selected parameters ensure a balance between efficiency and safety, providing optimal MRR while preserving the integrity of the machine and the workpiece.

In the context of the EDM machining of AISI D2 steel, the parameter Ip, representing the current pulse, is crucial for understanding the spark's energy. The energy of each spark in EDM is given by the equation $E = I^2 \times R \times t$, where E is the energy, I is the current, R is the resistance, and t is the time duration of the current pulse. This equation illustrates that the energy of each spark is proportional to the square of the current (I^2), indicating a quadratic relationship between current and spark energy. As the current pulse (Ip) increases, the energy of the spark is significantly enhanced due to this quadratic relationship, leading to a higher material removal rate (MRR) as more material is removed per spark. However, the influence of Ip on the overall process is relatively less profound compared to other parameters, as indicated by its delta value of 0.00297, placing it fourth in terms of significance. This lesser influence is attributed to the complex interplay of various factors in EDM, where other parameters may have a more dominant impact on the machining outcomes despite the critical role of Ip in determining spark energy.

Vg, representing the gap voltage between the tool and the workpiece in the EDM process, exhibits a nuanced relationship with MRR. An optimal voltage is crucial for efficient material removal. If the voltage is too low, it might not provide the requisite energy [15]. However, if it is excessively high, it can lead to arc discharges, detrimental to the machining process [55]. The voltage essentially determines the potential difference across the gap. This potential difference, in turn, dictates the energy of the spark. But one must tread cautiously, as excessively high voltages can introduce unstable discharging, causing inconsistencies in the material removal process.

Ton, the on-time duration of the pulse, is another significant parameter. By increasing Ton, the MRR generally witnesses an upsurge. The underlying reason is that the longer the pulse's duration, the more time the spark has at its disposal to erode the material. As a consequence, MRR increases. However, there is a caveat. If pulses are excessively prolonged, they might result in over-eroding, producing craters larger than desired [56].

In Table 4, T represents the duty cycle, a critical parameter in EDM. It refers to the percentage of time in a machining cycle during which the current is actually applied to the electrode. The values in Table 4 reflect the different duty cycle settings used in our experiments, ranging from 7% to 13%. The phrase 'duration of the machining cycle' refers to the total time for each experimental run, within which the duty cycle is applied as per the settings in Table 4. This clarification emphasizes the role of the duty cycle in determining the duration and efficiency of each machining operation. In contrast, an overly prolonged duty cycle can induce overheating or excessive erosion [57]. The paramount importance of T is underscored by its highest delta value of 0.02945, emphasizing the significance of maintaining a harmonious balance between spark energy and cooling intervals. It can be seen in Figure 4.

From the plot in Figure 5, it is evident that there are pronounced interactions among all the parameters. For instance, at high Vg levels, the material experiences increased energy, and when combined with different levels of Ip, there is a discernible change in the MRR. Similarly, low levels of Ton indicate shorter pulse durations which, when paired with varying T values, results in notable variations in the MRR. Such interactions suggest that individual parameter settings do not operate in isolation; instead, their combined effect influences the material removal rate. At elevated Vg levels, the potential difference across the EDM gap increases, resulting in a higher discharge energy that intensifies the erosion process. When the Ip parameter varies, it modulates the energy per discharge, directly influencing the MRR. The pulse-on time, Ton, correlates to the duration of energy application; shorter Ton leads to less energy transfer per cycle but may increase the number of discharges over time when T, the duty cycle, is varied. These parameters synergistically

affect the thermal and kinetic energies imparted to the workpiece, which are crucial in determining the MRR [58].
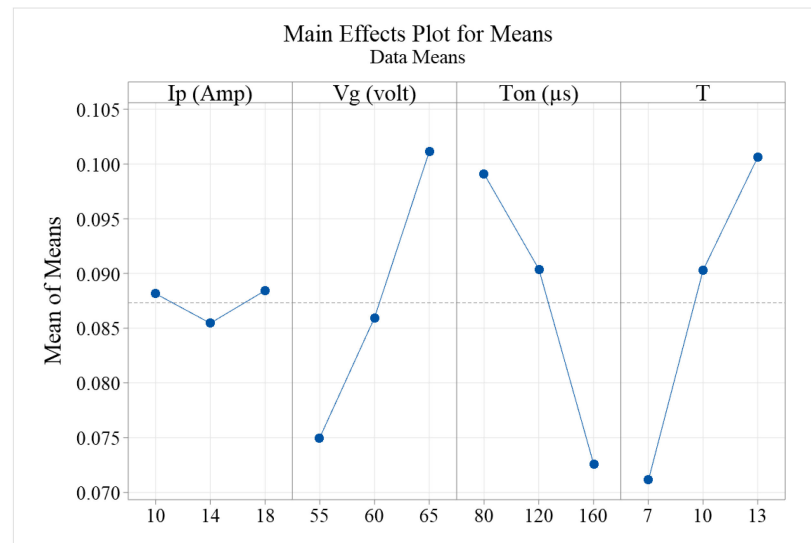

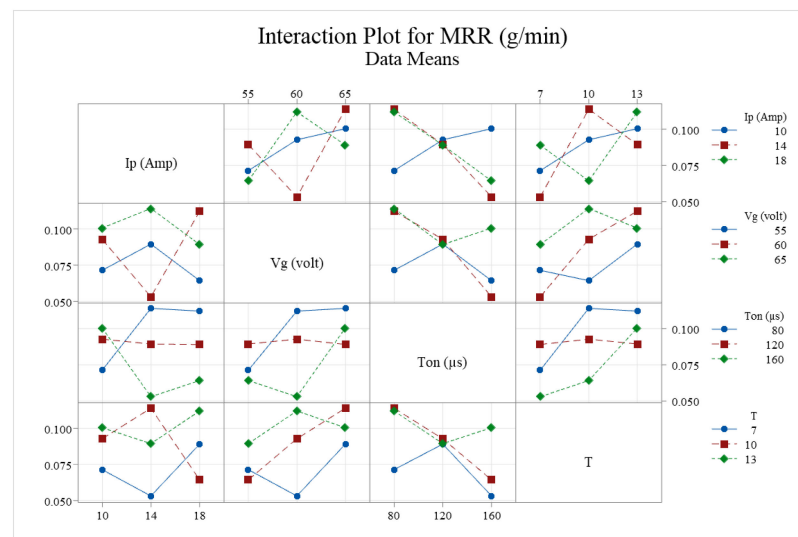**Figure 4.** MRR influenced by EDM equipment configurations.

Figure 5. Interactions on MRR influenced by EDM equipment configurations.

3.3. Effects of the EDM Parameters on EWR

The electrode wear rate (EWR) is another critical performance metric in the electrical discharge machining (EDM) process. It quantifies the rate at which the tool electrode wears out during the machining process. An optimal EWR ensures the precision and longevity of the tool electrode, resulting in consistent machining performance [59,60]. In the realm of this research, the EDM parameters, namely, Ip (Amp), Vg (volt), Ton (µs), and T, have been investigated for their influence on EWR.

A systematic study of the provided data tables and the interaction plot (as illustrated in Figure 6) reveals insightful patterns pertaining to the effects of these parameters on EWR. The highlights of these findings are detailed below:

- Ip (Amp): Representing the current pulse, this parameter has a prominent influence on EWR. Based on the provided response table, Ip exhibits a delta value of 0.001534. The rank associated with Ip is 2, signifying that it is the second most influential parameter

on EWR. When EDM is employed on AISI D2 steel, an increase in Ip generally leads to an accelerated wear rate of the electrode [61], attributed to the enhanced energy of each spark due to the heightened current.

- Vg (volt): This parameter, symbolizing the gap voltage between the tool and workpiece, has the most profound impact on EWR. With a delta value of 0.004705, Vg is ranked first in its influence on EWR. The relationship between Vg and EWR is intricate; a precise voltage is pivotal for maintaining tool wear at an optimal level. Elevated voltages can lead to intense spark energies, causing faster wear, whereas too low voltages might not facilitate the desired material removal, causing longer machine running times and subsequently more tool wear.
- Ton (μs): Denoting the on-time duration of the pulse, this parameter also showcases an influence on EWR. A delta value of 0.000537 places Ton in the third rank. When Ton is increased, there is an extended duration of spark activity, which might result in a higher wear rate. This is due to the extended time the spark interacts with both the workpiece and the tool electrode, enhancing material and tool wear, respectively [62].
- T: The duty cycle parameter, T, exhibits the least influence on EWR among the considered parameters. Its delta value stands at 0.000140, ranking it fourth. While T significantly impacts MRR, its influence on EWR is subdued. This underscores the fact that while longer duty cycles can result in enhanced material removal, they do not necessarily correlate to a proportionate increase in electrode wear [63].
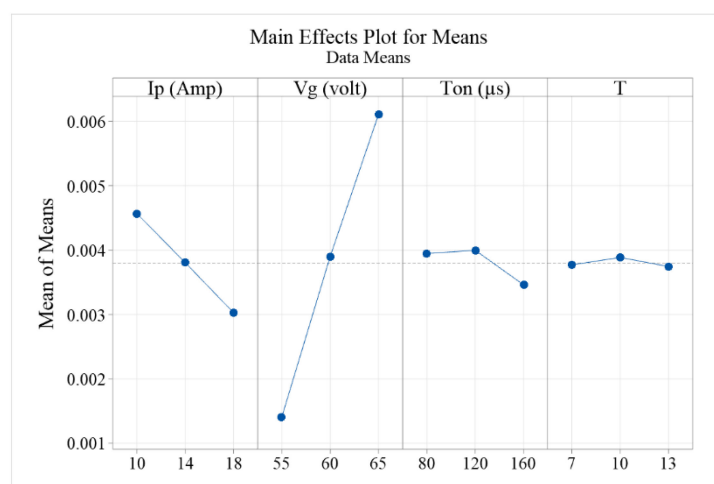

Figure 6. Interactions on EWR influenced by EDM equipment configurations.

From the plot presented in Figure 7, it is evident that there are pronounced interactions among the parameters, primarily between Ip, Vg, Ton, and T. Here is a detailed interpretation of the interactions:

- Ip (Amp) vs. Vg (volt): As Vg increases, the removal rate (EWR) for different levels of Ip shows varying behavior. Specifically, at an Ip of 10 Amps, there is a slight increase in EWR as Vg increases. However, at higher Ip levels (14 and 18 Amps), there is a decline in EWR with increasing Vg.
- Ip (Amp) vs. Ton (μs): The interaction between Ip and Ton indicates that for a constant Ip of 10 Amps, EWR slightly decreases as Ton increases. However, at Ip levels of 14 and 18 Amps, the EWR experiences a noticeable increase initially and then drops as Ton continues to increase.
- Ip (Amp) vs. T: The EWR displays a complex interaction pattern between Ip and T. For the lowest Ip of 10 Amps, the EWR initially increases and then dips as T rises. For the higher Ip levels (14 and 18 Amps), the EWR shows contrasting trends, increasing for Ip of 14 Amps and decreasing for Ip of 18 Amps with rising T.

- Vg (volt) vs. Ton (μs): For a constant Vg of 55 volts, the EWR increases as Ton rises. However, at Vg levels of 60 and 65 volts, the EWR decreases with increasing Ton.
- Vg (volt) vs. T: The interaction between Vg and T demonstrates varying behavior for different Vg levels. Notably, for a Vg of 55 volts, the EWR shows a minor decline as T increases, but at Vg levels of 60 and 65 volts, the EWR increases with rising T.
- Ton (μs) vs. T: For a constant Ton of 80 μs, there is a slight increase in EWR as T increases. At higher Ton values (120 and 160 μs), the EWR showcases opposing trends: a decrease for Ton of 120 μs and an increase for Ton of 160 μs with rising T.

In conclusion, the interactions depicted in the plot suggest that the parameter settings do not operate in isolation. Their combined effect considerably influences the EWR, and careful consideration is required when choosing parameter values to optimize the material removal process. Increased Ton times allow for more prolonged spark activity, potentially leading to greater electrode wear due to thermal loading. The interaction between Ton and T further elucidates this effect, with varying duty cycles affecting the frequency and duration of thermal exposure. The physical interpretation involves the consideration of thermal fatigue on the electrode material, where extended periods of high thermal stress may lead to increased wear rates, while shorter, more frequent cycles may mitigate this effect [64].
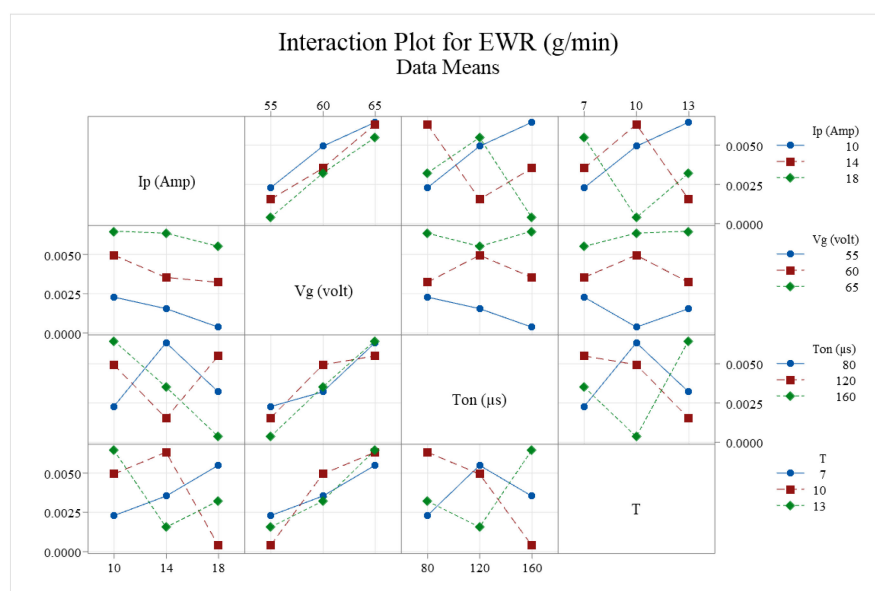

Figure 7. Interactions on EWR influenced by EDM equipment configurations.

3.4. Effects of the EDM Parameters on ROC

The radial overcut (ROC) is yet another essential performance metric in the electrical discharge machining (EDM) process. The ROC specifies the rate at which material is removed from the workpiece. For efficient and precise machining, achieving an optimal ROC is paramount. The EDM parameters under scrutiny in this research; i.e., Ip (Amp), Vg (volt), Ton (μs), and T have been analyzed for their implications on ROC.

A comprehensive examination of the interaction plot (depicted in the Figure 7) unveils discerning patterns associated with the effects of these parameters on ROC. The main insights from these observations are enumerated below:

- **Ip (Amp)**: The current pulse, symbolized by this parameter, exhibits a paramount effect on ROC. As per the data table, the delta value of Ip is 0.0425. With a ranking of 1, Ip stands out as the most influential parameter on ROC. Increasing Ip, particularly for materials like D2 steel, enhances the rate of cut, likely due to the amplified energy of each spark ensuing from an elevated current [65].

- **Vg (volt)**: Indicating the gap voltage between the electrode and the workpiece, this parameter is of significant importance to ROC. With its delta value recorded at 0.0342, Vg holds the second rank in terms of influence on ROC. Elevated Vg levels can bolster the spark energies, potentially leading to a more rapid material removal rate.
- **Ton (μs)**: Representing the on-time of each pulse, Ton too influences ROC. The delta value for Ton stands at 0.0154, placing it at the third rank. A lengthened Ton can augment spark interaction duration, possibly resulting in a heightened ROC, due to the extended interaction between the spark and the workpiece.
- **T**: This duty cycle parameter appears to have the least direct influence on ROC amongst the parameters considered. With a delta value of 0.0104, T is ranked fourth. A longer duty cycle might facilitate enhanced material removal without necessarily having a direct proportionate effect on the ROC.

From the interaction plot presented in Figure 8 (pertaining to ROC), there are evident interactions among the parameters, specifically between Ip, Vg, Ton, and T. The interactions can be interpreted as:

- **Ip (Amp) vs. Vg (volt)**: With increasing Vg, the ROC for various levels of Ip demonstrates distinct behavior. At an Ip level of 10 Amps, a rise in Vg corresponds to an incremental ROC. However, at elevated Ip levels (14 and 18 Amps), an increase in Vg results in a decline in ROC.
- **Ip (Amp) vs. Ton (μs)**: The interplay between Ip and Ton suggests that for an Ip of 10 Amps, ROC slightly dips with increasing Ton. In contrast, at Ip levels of 14 and 18 Amps, ROC initially escalates and subsequently reduces as Ton continues to rise.
- **Ip (Amp) vs. T**: ROC showcases an intricate interaction pattern between Ip and T. At the lowest Ip level of 10 Amps, ROC first ascends and then recedes as T augments. At more elevated Ip levels (14 and 18 Amps), ROC presents diverging tendencies—rising for an Ip of 14 Amps and dwindling for an Ip of 18 Amps as T surges.
- **Vg (volt) vs. Ton (μs)**: For a consistent Vg of 55 volts, ROC surges as Ton swells. Nonetheless, at Vg values of 60 and 65 volts, ROC declines with increasing Ton.
- **Vg (volt) vs. T**: The interrelation between Vg and T displays variable dynamics for different Vg values. Notably, at a Vg of 55 volts, ROC marginally reduces as T augments, but at Vg measurements of 60 and 65 volts, ROC advances with an upswing in T.
- **Ton (μs) vs. T**: At a stable Ton of 80 μs, there is a subtle elevation in ROC as T rises. At more considerable Ton measurements (120 and 160 μs), ROC reveals contradictory trends: a decline for Ton of 120 μs and an upturn for Ton of 160 μs with an escalation in T.
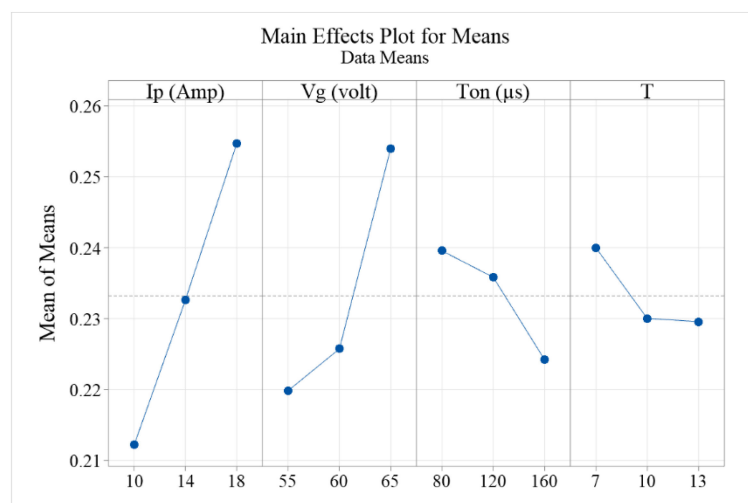

Figure 8. ROC influenced by EDM equipment configurations.

To encapsulate, the interactions outlined in the plots in Figure 9 accentuate that the parameter settings are interdependent. Their synergistic impact significantly determines ROC, necessitating meticulous consideration when calibrating parameter values to fine-tune the material removal process. As Ip increases, so does the thermal penetration, leading to a wider ROC. The Vg parameter's effect on ROC can be interpreted as the control over the spark gap distance, which affects discharge stability and energy concentration. A stable and appropriate Vg is essential for achieving a controlled ROC, providing a balance between cutting efficiency and precision [66].
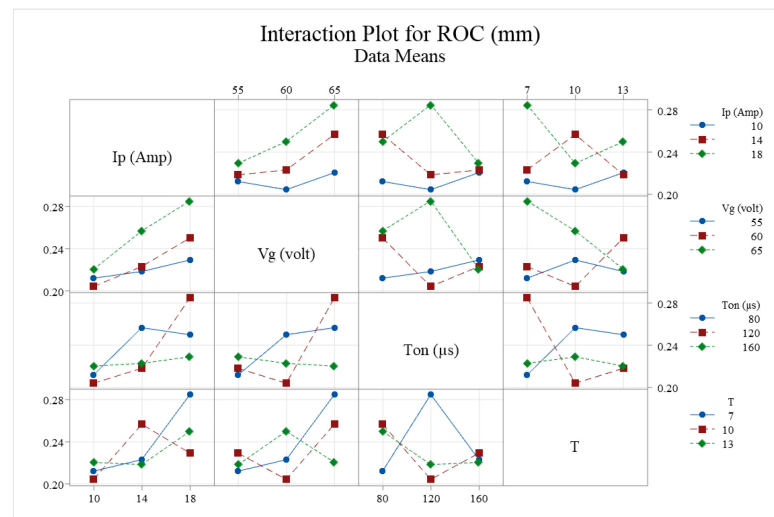

Figure 9. Interactions on ROC influenced by EDM equipment configurations.

3.5. Optimal Parameters for MRR, EWR, and ROC Selection

Tables A1–A3 shows parametric S/N responses. Given the graphical representation (provided in Figure 10) of the main effects plot for signal-to-noise (S/N) ratios pertaining to the EDM machine parameters, it is evident that the parameters under examination are Ip (Amp), Vg (volt), Ton (μs), and T. As the provided graph reveals, specific trends and patterns can be discerned which can inform optimal parameter settings for attaining desired results.
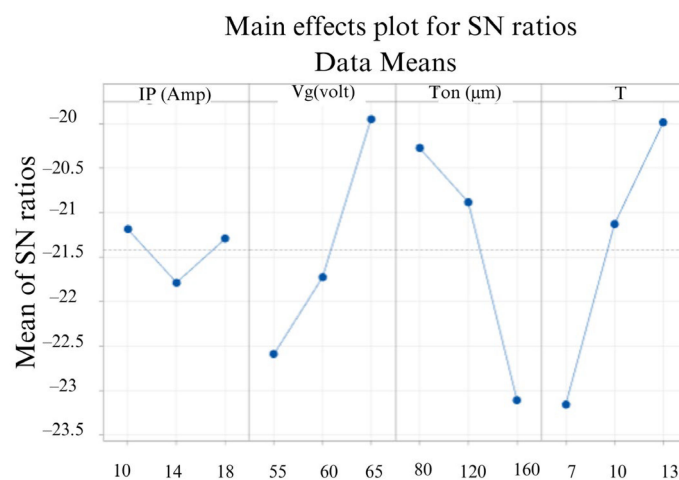

Figure 10. Mean S/N values for MRR of AISI D2 steel.

Upon examination of the plot and juxtaposing it with the textual information provided, the following insights can be deduced:

1. **Ip (Amp)**: The signal-to-noise ratio for this parameter shows a moderate change across the levels. The highest mean S/N ratio appears at the 18 Amp setting.
2. **Vg (volt)**: The mean S/N ratio demonstrates a substantial increase as the Vg (volt) value rises, indicating its importance in the EDM process.
3. **Ton (µs)**: This parameter exhibits a prominent dip around 120 µs before rising sharply again, suggesting that there might be specific optimal regions around 80 µs and 160 µs.
4. **T**: The trend for T is upward, indicating that a higher setting for T results in a superior S/N ratio.

Referring to the provided response table for signal-to-noise ratios, it can be discerned that among all the parameters, T demonstrates the highest delta value of 3.16, subsequently ranked as 1. This suggests that T has the most significant impact on the process. Following T, the parameters Ton (µs) and Vg (volt) have delta values of 2.83 and 2.64, respectively, indicating their significance in descending order. Ip (Amp), with a delta value of 0.60, is ranked 4, suggesting its lesser impact compared to the other parameters.

From Figure 11, the main effects plot for signal-to-noise (S/N) ratios depicts the response of the EDM process parameters: Ip (Amp), Vg (volt), Ton (µs), and T. A discernible trend suggests that Vg (volt) has the most significant impact, with its S/N ratio decreasing markedly as the voltage increases. This is supported by the response table, which ranks Vg (volt) as the most influential parameter with the highest delta value of 14.91. Following Vg (volt), the parameters are ranked in descending order of impact as Ip (Amp) with a delta of 6.96, Ton (µs) with a delta of 4.92, and T with a delta of 3.87. The trends and data reveal that adjustments in these parameters, particularly Vg (volt), can considerably influence the S/N ratio, and thus the performance, of the EDM process.
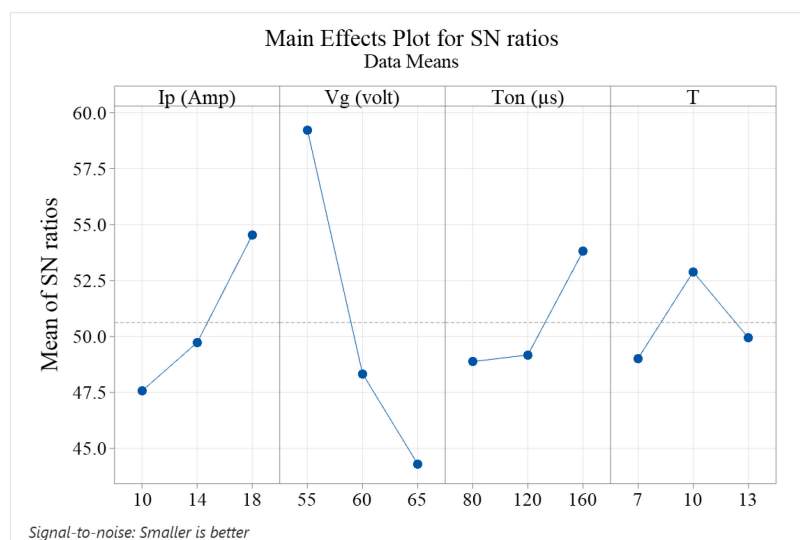
Figure 11. Mean S/N values for EWR of D2 steel.

From Figure 12, The graph distinctly shows the response of each parameter in relation to the mean of S/N ratios. Upon detailed analysis of the graph and table:

1. The parameter **Ip (Amp)** shows a decreasing trend in the S/N ratio as the current increases. From the response table, the delta value for Ip (Amp) is given as 1.56, making it the most influential parameter. Thus, it is ranked first in terms of its impact on the S/N ratio.
2. The next parameter, **Vg (volt)**, also exhibits a decreasing trend in its S/N ratio as the voltage increases. The response table corroborates this by providing a delta value of 1.21 for Vg (volt), ranking it as the second most influential parameter.

3. **Ton (µs)** shows an initially decreasing S/N ratio, but there is an increase observed at the third data point. With a delta value of 0.55 from the response table, it is ranked third.

4. Lastly, **T** maintains a relatively stable S/N ratio across the range. It has the smallest delta value of 0.33, ranking it fourth in terms of impact on the S/N ratio.
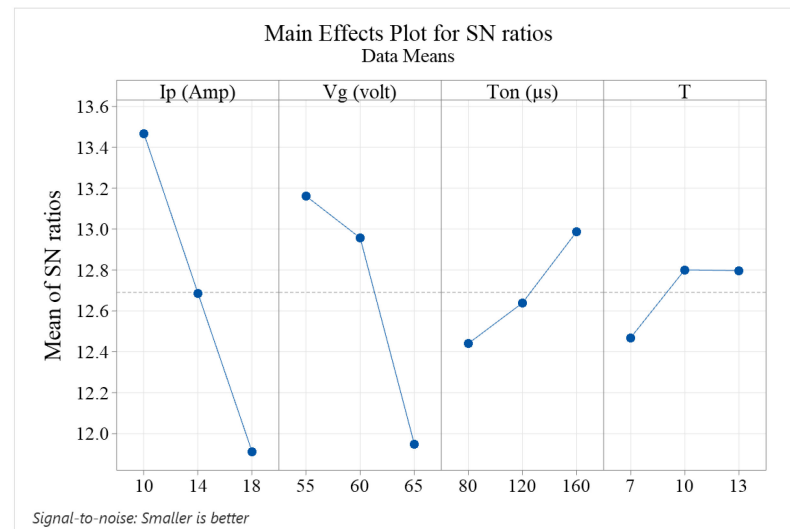

Figure 12. Mean S/N values for ROC of D2 steel.

3.6. Validation Test

It is essential to conduct confirmation experiments to verify the projected ideal conditions through Taguchi's method. Equation (4) [67] was employed to determine the projected S/N ratio ($\varepsilon_{predicted}$) and to gauge and evaluate the responses under the predicted optimal conditions for the response parameters: MRR, EWR, and ROC.

$$\varepsilon_{predicted} = \varepsilon_l + \sum_{i=0}^{x} \varepsilon_0 - \varepsilon_n \tag{4}$$

ε_n = total S/N ratio;
ε_0 = mean S/N ratio (at optimum point);
x = input number of EDM parameters.

Table A4 for MRR, Table A5 for EWR, and Table A6 for ROC detail the results of the confirmation experiments conducted at the optimal EDM parameters projected by Taguchi. When optimal conditions for the EDM process are applied, performance attributes of MRR, EWR, and ROC demonstrate improvement. As can be seen in Table A6, the predicted and optimal conditions for each parameter have closely matching S/N ratios. Specifically:

1. **MRR (g/min)**: At the optimal EDM conditions, the S/N ratio improved by 4.02 dB when compared to initial parameter values. The verification experiments demonstrate that MRR reduced by 29.13% under Taguchi's predicted optimal conditions compared to the baseline parameters.

2. **EWR (g/min)**: The S/N ratio showed an improvement of 10.35 dB under optimal EDM conditions. Furthermore, the EWR was reduced by 33.33% under the optimal conditions in comparison to the preliminary settings.

3. **ROC (mm)**: The improvement in the S/N ratio for ROC was 2.20 dB under the optimal EDM conditions. ROC increased by 28.57% when comparing the baseline parameters to Taguchi's predicted ideal conditions.

3.7. Comparison of Current Findings with the Published Work

Table 4 lists the studies that have been conducted on micro- and macro-hole drilling in CFRP EDM. Few studies have been performed on hole making that goes deeper than 5 mm. For validation purposes, a distinction was made between the current study and the existing literature. In comparison to the findings of the literature currently in publication, the current study yields the highest penetration limit of 7 mm with a machining diameter of 9.89 mm in EDM macro-hole drilling.

Table 4. Comparison with the published literature.

Citation	Machining Type: Micro (mic)/Macro (mac)	Hole Type: Blind (Hb) or Through (Ht)	Electrode Type: Copper (Cu), Graphite (C), Tungsten Carbide (WC), Aluminum (Al), and Brass (Br)	Machining Diameter (mm)	Penetration Limit (mm)
[68]	Mac	Hb	Cu and C	9.95	1.0
[69]	Mac	Hb	Cu	4.40	1.0
[70]	Mac	Hb	Cu	7.79	1.0
[71]	Mac	Hb	Cu	1.99	1.0
[72]	Mac	Ht	Cu	5.86	5.0
[73]	Mac	Ht	C	5.97	1.80
[74]	Mac	Ht	Cu and C	5.55	1.80
[75]	Mic	Hb	WC	0.49	0.20
[76]	Mic	Hb	WC	0.10	1.20
[77]	Mac	Ht	Cu	7.89	6.0
[78]	Mac	Hb	Copper (Cu), Aluminum (Al), Graphite (C), and Brass (Br),	15	1
[79]	Mic	Hb	Cu	0.49	0.250
Current work	Mac	Ht	Cu	9.89	7.0

4. ANOVA for MRR, EWR, and ROC

The ANOVA identifies the most important FFF tuning knob to optimize performance. ANOVA analysis played a crucial role in identifying the hierarchy of influential factors on machining attributes. Notably, duty cycle emerged as the most influential parameter on material removal rate, followed by pulse duration, gap voltage, and peak current. These insights are now clearly presented in Tables 5–7. Tables 5–7 display the results of the ANOVA tests conducted on Ra, Rq and PT, PE, and T. Table 5 demonstrates that amongst the EDM machine parameters, T exerts the most significant influence on MRR, followed by Ton (µs), Vg (volt), and Ip (Amp). In descending order, the effects of T, Ton (µs), Vg (volt), and Ip (Amp) on MRR are 37.31%, 30.25%, 29.42%, and 0.00%, respectively.

Table 5. ANOVA for MRR of AISI D2 steel.

Scheme	DF	Seq SS	Contribution	Adj SS	Adj MS	F-Value	*p*-Value	Residuals	SD
Regression	4	0.003382	96.98%	0.003382	0.000846	32.13	0.003	−0.0013423	−0.55508
Ip (Amp)	1	0.000000	0.00%	0.000000	0.000000	0.00	0.950	0.0055127	1.26450
Vg (volt)	1	0.001026	29.42%	0.001026	0.001026	38.99	0.003	−0.0013423	−0.55508
Ton (µs)	1	0.001055	30.25%	0.001055	0.001055	40.08	0.003	0.0003797	0.09930
T	1	0.001301	37.31%	0.001301	0.001301	49.45	0.002	−0.0062793	−1.64226
Error	4	0.000105	3.02%	0.000105	0.000026			0.0002437	0.06373
Total	8	0.003488	100.00%					0.0030717	0.96018

Table 6. ANOVA table for the EWR of D2 steel.

Source	DF	Seq SS	Contribution	Adj SS	Adj MS	F-Value	*p*-Value	Residuals	SD
Regression	4	0.000037	99.34%	0.000037	0.000009	150.78	0.000	−0.0001908	−1.63239
Ip (Amp)	1	0.000004	9.46%	0.000004	0.000004	57.42	0.002	0.0003737	1.77286
Vg (volt)	1	0.000033	88.92%	0.000033	0.000033	539.88	0.000	−0.0001908	−1.63239
Ton (μs)	1	0.000000	0.96%	0.000000	0.000000	5.80	0.074	0.0001105	0.59789
T	1	0.000000	0.00%	0.000000	0.000000	0.02	0.903	−0.0000389	−0.21032
Error	4	0.000000	0.66%	0.000000	0.000000			−0.0000556	−0.30066
Total	8	0.000037	100.00%					−0.0000636	−0.41130

Table 7. ANOVA table for the ROC of D2 Steel.

Source	DF	Seq SS	Contribution	Adj SS	Adj MS	F-Value	*p*-Value	Residuals	SD
Regression	4	0.004986	93.82%	0.004986	0.001246	15.18	0.011	0.0042667	0.99877
Ip (Amp)	1	0.002714	51.07%	0.002714	0.002714	33.04	0.005	−0.0077333	−1.00415
Vg (volt)	1	0.001754	33.02%	0.001754	0.001754	21.36	0.010	0.0042667	0.99877
Ton (μs)	1	0.000354	6.67%	0.000354	0.000354	4.31	0.106	0.0074167	1.09803
T	1	0.000163	3.07%	0.000163	0.000163	1.99	0.231	−0.0077333	−1.14491
Error	4	0.000328	6.18%	0.000328	0.000082	-	-	−0.0012833	−0.19000
Total	8	0.005314	100.00%	-	-	-	-	−0.0004833	−0.08553

Table 6 demonstrates that amongst the EDM machine parameters, Vg (volt) exerts the most significant influence on MRR, followed by Ip (Amp), Ton (μs), and T. In descending order, the effects of Vg (volt), Ip (Amp), Ton (μs), and T on EWR are 88.92%, 9.46%, 0.96%, and 0.00%, respectively.

Table 7 demonstrates that amongst the EDM machine parameters, Ip (Amp) exerts the most significant influence on MRR, followed by Vg (volt), Ton (μs), and T. In descending order, the effects of Ip (Amp), Vg (volt), Ton (μs), and T on MRR are 51.07%, 33.02%, 6.67%, and 3.07%, respectively.

5. Mathematical Modeling

Utilizing Minitab 21.3, a regression evaluation was performed, facilitating the creation of predictive models for the MRR, EWR, and ROC variables based on parameters like Ip (Amp), Vg (volt), Ton (μs), and T. All response variables remained unaltered. The coefficient of determination, R^2 [80], is an essential metric to evaluate the performance of established models [81]. A value nearing one signifies a strong correlation between the dependent and independent variables [82,83]. The models were evaluated with the provided summaries:

For the MRR model (Figure 13), an R^2 value of 96.98% implies that the model accounts for approximately 96.98% of the variability in the data.

To assess the significance of a model's coefficients, one should inspect the residual plots [84]. A prominent coefficient, complemented by a linear trajectory in the residual plot, suggests that the errors of the model are distributed in a regular manner [85].

For EWR (Figure 14), the R^2 value is even more impressive at 99.34%, suggesting almost complete congruence between the dependent and independent variables. Lastly, the ROC model (Figure 15) has an R^2 value of 93.82%, showcasing its substantial efficiency in predicting the data variability.

The constructed frameworks underwent a sequence of compliance assessments depicted in Table 8 The evaluations' results were selected randomly from the structure of L9. The validation findings indicated that, within the stipulated parameter boundaries, the anticipated values from the framework and the empirical information were in tight concordance. This analysis was instrumental in developing predictive models for MRR, EWR, and ROC. We have elucidated the coefficients of determination (R^2) for each model, affirming their robustness in predicting optimal machining conditions.
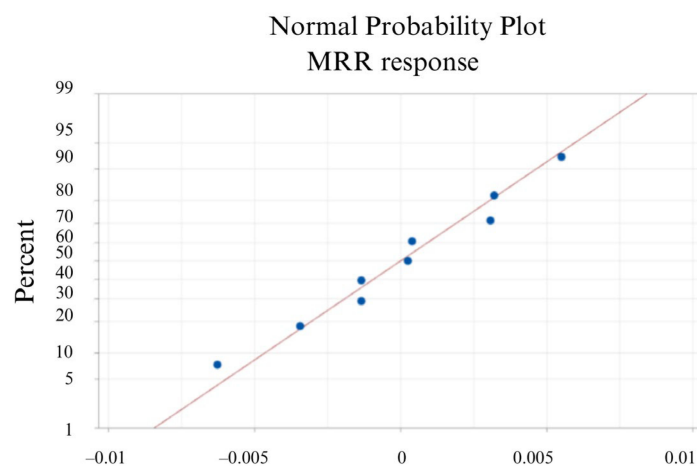
Normal Probability Plot
MRR response

Figure 13. Graphs delineating the standard probability distribution for MRR.

Normal Probability Plot
EWR response
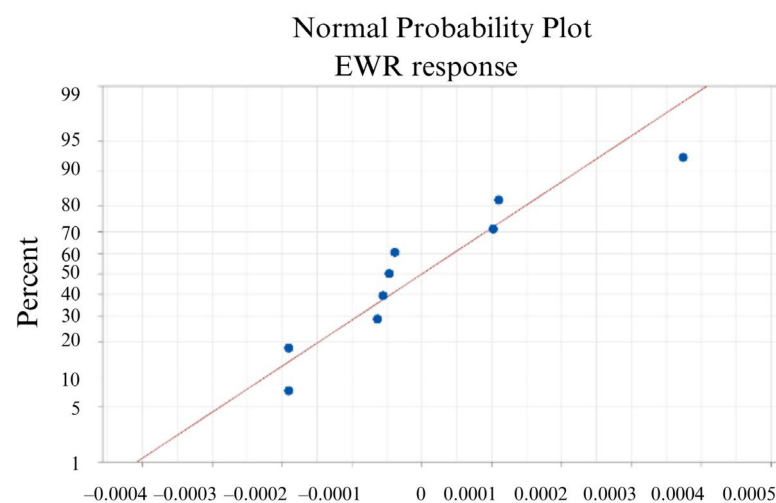
Figure 14. Graphs delineating the standard probability distribution for EWR.

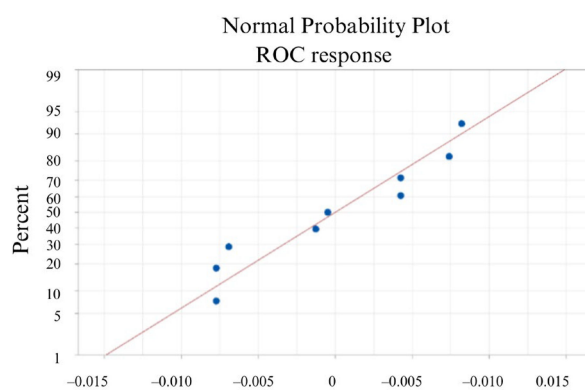## Normal Probability Plot
ROC response

Figure 15. Graphs delineating the standard probability distribution for ROC.

Table 8. Confirmation model for verification.

Run	Experimented			Predicted			Percentage Difference		
-	MRR	EWR	ROC	MRR	EWR	ROC	MRR	EWR	ROC
6	0.113906	0.00634	0.2567	0.114	0.0064	0.258	0.08	0.95	0.51
9	0.089022	0.0055	0.285	0.086	0.00540	0.277	3.39	1.82	2.81

6. Conclusions and Future Directions

The following are the key findings of the investigation into the electrical discharge machining (EDM) of AISI D2 steel:

- A meticulous examination of the effects of various EDM parameters on material removal rate (MRR), electrode wear rate (EWR), and radial overcut (ROC) was conducted. Notably, the duty cycle (T) was identified as the most critical parameter, significantly influencing MRR, as indicated by the highest delta value of 0.02945.
- The pulse duration (Ton) emerged as the second most significant factor, with a delta value of 0.02652, affecting MRR. This highlights the importance of the on-time duration of the pulse in the EDM process.
- Gap voltage (Vg) also showed a considerable impact on MRR, evidenced by a delta value of 0.02615, ranking third in terms of its influence.
- Peak current (Ip), with a delta value of 0.00297, demonstrated a notable but lesser influence on MRR, placing it fourth in significance.
- Based on these findings, predictive models have been developed to determine the ideal EDM conditions. These models are instrumental in forecasting optimal machining scenarios, thereby reducing the necessity for extensive preliminary testing.
- The insights from this study provide a solid foundation for future academic research and practical implementation in the field of EDM. They offer valuable guidance for refining EDM operations, particularly in terms of efficiency, reduced electrode wear, and improved accuracy. Such advancements could translate into economic efficiencies and elevated manufacturing standards.
- The statistical treatment of our findings not only substantiates the influence of parameters like duty cycle and pulse duration on machining attributes but also aids in the development of predictive models. These models are vital for forecasting optimal machining conditions, thereby reducing the need for extensive preliminary testing.

Future Recommendations

- It was discovered that the output responses are contradictory. Thus, it is suggested that future work focus on mathematical modeling using optimization and neural network-based numerical models. Furthermore, more thorough research is needed to fully understand the microstructural analysis of AISI D2 steel in EDM.
- Further exploration of variables related to AISI D2 steel in the EDM operation is recommended, culminating in the formulation of comprehensive industrial blueprints.
- Scrutinize the physical attributes of D2 metal under diverse EDM configurations.
- Delve deeper into enhancement techniques to amplify machining efficacy, potentially amalgamating approaches like the response surface methodology.

Author Contributions: Conceptualization, A.H.; Methodology, A.H., R.T.M., A.M.K.; Validation, A.H., R.T.M.; Formal analysis, A.H. and A.M.K.; Investigation, A.H.; Writing—original draft preparation, A.H.; Funding acquisition, A.H., A.M.K., S.A.; Supervision, R.T.M.; Writing—review and editing, R.T.M. and A.M.K.; Data curation, S.A.; Visualization, S.A. All authors have read and agreed to the published version of the manuscript.

Conflicts of Interest: The authors declare no conflict of interest.

Appendix A

Table A1. Mean response table of S/N ratio for MRR of AISI D2 steel.

Level	Ip (Amp)	Vg (volt)	Ton (µs)	T
1	−21.19	−22.59	−20.27	−23.15
2	−21.78	−21.73	−20.88	−21.13
3	−21.29	−19.95	−23.11	−19.99
Delta	0.60	2.64	2.83	3.16
Rank	4	3	2	1

Table A2. Mean response table of S/N ratio for EWR of AISI D2 steel.

Level	Ip (Amp)	Vg (volt)	Ton (µs)	T
1	47.58	59.22	48.88	49.03
2	49.74	48.34	49.18	52.89
3	54.55	44.31	53.81	49.95
Delta	6.96	14.91	4.92	3.87
Rank	2	1	3	4

Table A3. Mean response table of S/N ratio for ROC of AISI D2 steel.

Level	Ip (Amp)	Vg (volt)	Ton (µs)	T
1	13.47	13.16	12.44	12.47
2	12.69	12.96	12.64	12.80
3	11.91	11.95	12.99	12.80
Delta	1.56	1.21	0.55	0.33
Rank	1	2	3	4

Table A4. The validation test outcomes for MRR of AISI D2 steel.

	Preliminary Parameters		Optimum Parameters	
	Predicted	**Experimental**	**Predicted**	**Experimental**
Level	Ip-S2 Vg-S2 Ton-S2 T-S2	Ip-S2 Vg-S2 Ton-S2 T-S2	Ip-S1 Vg-S3 Ton-S1 T-S3	Ip-S1 Vg-S3 Ton-S1 T-S3
MRR (g/min)		0.09		0.127
S/N ratio (dB) MRR (g/min)	−21.25	−21.26	−17.22	−17.24
S/N ratio (dB) improvement for MRR (g/min)	4.02			
% increment in MRR (g/min)	29.13			

Table A5. The validation test outcomes for EWR of AISI D2 steel.

	Preliminary Parameters		Optimum Parameters	
	Predicted	**Experimental**	**Predicted**	**Experimental**
Level	Ip-S2 Vg-S2 Ton-S2 T-S2	Ip-S2 Vg-S2 Ton-S2 T-S2	Ip-S1 Vg-S3 Ton-S1 T-S1	Ip-S1 Vg-S3 Ton-S1 T-S1
EWR (g/min)		0.004		0.006
S/N ratio (dB) for EWR (g/min)	48.273	48.29	37.92	37.94
S/N ratio (dB) improvement for EWR (g/min)	10.35			
% Reduction in EWR (g/min)	33.33			

Table A6. The validation test outcomes for ROC of AISI D2 steel.

	Preliminary Parameters		Optimum Parameters	
	Predicted	Experimented	Predicted	Experiment
Level	Ip-S2 Vg-S2 Ton-S2 T-S2	Ip-S2 Vg-S2 Ton-S2 T-S2	Ip-S3 Vg-S3 Ton-S1 T-S1	Ip-S3 Vg-S3 Ton-S1 T-S1
ROC (mm)		0.224		0.288
S/N ratio (dB) for ROC (mm)	13.01	13.03	10.78	10.83
S/N ratio (dB) improvement for ROC (mm)	2.20			
% reduction in ROC (mm)	28.57			

References

1. Karmiris-Obratański, P.; Zagórski, K.; Papazoglou, E.L.; Markopoulos, A.P. Surface Texture and Integrity of Electrical Discharged Machined Titanium Alloy. *Int. J. Adv. Manuf. Technol.* **2021**, *115*, 733–747. [CrossRef]
2. Tian, H.; Wang, K.; Shui, Z.; Ali Raza, M.; Xiao, H.; Que, M.; Zhu, L.; Chen, X. Enhanced CO_2 Electroreduction on Co Active Site of Cobalt Phthalocyanine by Electronic Effect. *Mater. Lett.* **2022**, *310*, 131482. [CrossRef]
3. Ablyaz, T.R.; Shlykov, E.S.; Muratov, K.R. Improving the Efficiency of Electrical Discharge Machining of Special-Purpose Products with Composite Electrode Tools. *Materials* **2021**, *14*, 6105. [CrossRef] [PubMed]
4. Rehan, M.; Khan, S.A.; Naveed, R.; Usman, M.; Anwar, S.; AlFaify, A.Y.; Pruncu, C.I.; Lamberti, L. Experimental Investigation of the Influence of Wire Offset and Composition on Complex Profile WEDM of Ti6Al4V Using Trim-Pass Strategy. *Int. J. Adv. Manuf. Technol.* **2023**, *127*, 1209–1224. [CrossRef]
5. Liao, D.; Zhu, S.-P.; Keshtegar, B.; Qian, G.; Wang, Q. Probabilistic Framework for Fatigue Life Assessment of Notched Components under Size Effects. *Int. J. Mech. Sci.* **2020**, *181*, 105685. [CrossRef]
6. Niu, X.; Zhu, S.-P.; He, J.-C.; Liao, D.; Correia, J.A.F.O.; Berto, F.; Wang, Q. Defect Tolerant Fatigue Assessment of AM Materials: Size Effect and Probabilistic Prospects. *Int. J. Fatigue* **2022**, *160*, 106884. [CrossRef]
7. Babu, N.B.K.; Ramesh, T.; Muthukumaran, S. Physical, Tribological and Viscoelastic Behavior of Machining Wear Debris Powder Reinforced Epoxy Composites. *J. Clean. Prod.* **2020**, *272*, 122786. [CrossRef]
8. Raza, M.A.; Cai, W.; Tian, H.; Que, M.; Zhu, L.; Chen, X. Hierarchical Flower-like Ternary Composite of $NiFeCr/PCN/CeO_2$ towards Efficient Photocatalytic Reduction of CO_2. *J. Phys. Chem. Solids* **2022**, *171*, 111027. [CrossRef]
9. Senthilkumar, C.; Nandakumar, C. Optimization of Wire Electro Discharge Machining Parameters Using Principal Component Analysis. *Int. J. Syst. Assur. Eng. Manag.* **2023**, *14*, 1040–1048. [CrossRef]
10. Zhang, Z.; Chen, J.; Wang, J.; Han, Y.; Yu, Z.; Wang, Q.; Zhang, P.; Yang, S. Effects of Solder Thickness on Interface Behavior and Nanoindentation Characteristics in Cu/Sn/Cu Microbumps. *Weld. World* **2022**, *66*, 973–983. [CrossRef]
11. Guo, K.; Gou, G.; Lv, H.; Shan, M. Jointing of CFRP/5083 Aluminum Alloy by Induction Brazing: Processing, Connecting Mechanism, and Fatigue Performance. *Coatings* **2022**, *12*, 1559. [CrossRef]
12. Bose, S.; Nandi, T. Experimental Investigation of WEDM on Titanium Hybrid Composite Reinforced with Boron Powder: A Novel Approach. *Eur. Phys. J. Plus* **2020**, *135*, 914. [CrossRef]
13. Al-Amin, M.; Abdul-Rani, A.M.; Danish, M.; Thompson, H.M.; Aliyu, A.A.A.; Hastuty, S.; Zohura, F.T.; Bryant, M.G.; Rubaiee, S.; Rao, T.V.V.L.N. Assessment of PM-EDM Cycle Factors Influence on Machining Responses and Surface Properties of Biomaterials: A Comprehensive Review. *Precis. Eng.-J. Int. Soc. Precis. Eng. Nanotechnol.* **2020**, *66*, 531–549. [CrossRef]
14. Rashid, M.A.N.; Saleh, T.; Noor, W.I.; Ali, M.S.M. Effect of Laser Parameters on Sequential Laser Beam Micromachining and Micro Electro-Discharge Machining. *Int. J. Adv. Manuf. Technol.* **2021**, *114*, 709–723. [CrossRef]
15. Pragadish, N.; Kaliappan, S.; Subramanian, M.; Natrayan, L.; Prakash, K.S.; Subbiah, R.; Kumar, T.C.A. Optimization of Cardanol Oil Dielectric-Activated EDM Process Parameters in Machining of Silicon Steel. *Biomass Convers. Biorefin.* **2022**, *13*, 14087–14096. [CrossRef]
16. Fu, Z.H.; Yang, B.J.; Shan, M.L.; Li, T.; Zhu, Z.Y.; Ma, C.P.; Zhang, X.; Gou, G.Q.; Wang, Z.R.; Gao, W. Hydrogen Embrittlement Behavior of SUS301L-MT Stainless Steel Laser-Arc Hybrid Welded Joint Localized Zones. *Corros. Sci.* **2020**, *164*, 108337. [CrossRef]
17. Zhu, Z.Y.; Liu, Y.L.; Gou, G.Q.; Gao, W.; Chen, J. Effect of Heat Input on Interfacial Characterization of the Butter Joint of Hot-Rolling CP-Ti/Q235 Bimetallic Sheets by Laser+ CMT. *Sci. Rep.* **2021**, *11*, 10020. [CrossRef] [PubMed]
18. Gao, Q.; Ding, Z.; Liao, W.-H. Effective Elastic Properties of Irregular Auxetic Structures. *Compos. Struct.* **2022**, *287*, 115269. [CrossRef]
19. Asif, N.; Saleem, M.Q.; Farooq, M.U. Performance Evaluation of Surfactant Mixed Dielectric and Process Optimization for Electrical Discharge Machining of Titanium Alloy Ti6Al4V. *CIRP J. Manuf. Sci. Technol.* **2023**, *43*, 42–56. [CrossRef]
20. Singh, R.; Yadav, V.K.; Dvivedi, A.; Kumar, P. Evaluating the Feasibility of Using Biodegradable Castor Oil as a Dielectric Medium during Micro-Electrical Discharge Machining of Inconel 718. *J. Mater. Eng. Perform.* **2023**, *32*, 6465–6477. [CrossRef]
21. Suresh, K.; Karuppasamy, K.; Palani, S.; Krishnan, S.S.J.; Maridurai, T. Effect of Silane Treated Wheat Husk Biosilica (WHB) Deionized Water Dielectric on EDM Drilling of Ti-6Al-4 V Alloy. *Silicon* **2022**, *14*, 9143–9151. [CrossRef]

22. Dutta, S.; Singh, A.K.; Paul, B.; Paswan, M.K. Machining of Shape-Memory Alloys Using Electrical Discharge Machining with an Elaborate Study of Optimization Approaches: A Review. *J. Braz. Soc. Mech. Sci. Eng.* **2022**, *44*, 557. [CrossRef]
23. Arif, U.; Khan, I.A.; Hassan, F. Green and Sustainable Electric Discharge Machining: A Review. *Adv. Mater. Process. Technol.* **2022**, 1–75. [CrossRef]
24. Jadam, T.; Datta, S. Machinability of Ti-5Al-2.5Sn for Electro-Discharge Machining: An Experimental Investigation. *Sadhana-Acad. Proc. Eng. Sci.* **2020**, *45*, 238. [CrossRef]
25. Thejasree, P.; Natarajan, M. Applications of Hybrid Artificial Intelligence Tool in Wire Electro Discharge Machining of 7075 Aluminium Alloy. *Int. J. Interact. Des. Manuf.—IJIDEM* **2023**, 1–12. [CrossRef]
26. Shastri, A.S.; Nargundkar, A.; Kulkarni, A.J.; Sharma, K.K. Multi-Cohort Intelligence Algorithm for Solving Advanced Manufacturing Process Problems. *Neural Comput. Appl.* **2020**, *32*, 15055–15075. [CrossRef]
27. Zhu, Q.; Chen, J.; Gou, G.; Chen, H.; Li, P. Ameliorated Longitudinal Critically Refracted—Attenuation Velocity Method for Welding Residual Stress Measurement. *J. Mater. Process. Technol.* **2017**, *246*, 267–275. [CrossRef]
28. Chen, Y.; Sun, S.; Zhang, T.; Zhou, X.; Li, S. Effects of Post-Weld Heat Treatment on the Microstructure and Mechanical Properties of Laser-Welded NiTi/304SS Joint with Ni Filler. *Mater. Sci. Eng. A* **2020**, *771*, 138545. [CrossRef]
29. Yu, H.; Zhang, J.; Fang, M.; Ma, T.; Wang, B.; Zhang, Z.; Hu, Z.; Li, H.; Cao, X.; Ding, C. Bio-Inspired Strip-Shaped Composite Composed of Glass Fabric and Waste Selvedge from A. Pernyi Silk for Lightweight and High-Impact Applications. *Compos. Part A Appl. Sci. Manuf.* **2023**, *174*, 107715. [CrossRef]
30. Al-Amin, M.; Rani, A.M.A.; Aliyu, A.A.A.; Razak, M.A.A.; Hastuty, S.; Bryant, M.G. Powder Mixed-EDM for Potential Biomedical Applications: A Critical Review. *Mater. Manuf. Process.* **2020**, *35*, 1789–1811. [CrossRef]
31. Xing, Q.; Yao, Z.; Zhang, Q. Effects of Processing Parameters on Processing Performances of Ultrasonic Vibration-Assisted Micro-EDM. *Int. J. Adv. Manuf. Technol.* **2021**, *112*, 71–86. [CrossRef]
32. Phate, M.; Toney, S.; Phate, V. Modelling and Investigating the Impact of EDM Parameters on Surface Roughness in EDM of Al/Cu/Ni Alloy. *Aust. J. Mech. Eng.* **2022**, *20*, 1226–1239. [CrossRef]
33. Papazoglou, E.L.; Karmiris-Obratański, P.; Karkalos, N.E.; Thangaraj, M.; Markopoulos, A.P. Theoretical and Experimental Analysis of Plasma Radius Expansion Model in EDM: A Comprehensive Study. *Int. J. Adv. Manuf. Technol.* **2023**, *126*, 2429–2444. [CrossRef]
34. Bayki, S.; Mujumdar, S. A 1D Model for Prediction of Dry Electrical Discharge Machining (Dry-EDM) Plasma Characteristics. *J. Manuf. Process.* **2023**, *102*, 417–428. [CrossRef]
35. Liu, C.; Li, Q.; Yang, X. Analysis of Arc Plasma Characteristics and Energy Distribution in EDM Based on Two-Temperature Model. *Precis. Eng.* **2023**, *83*, 204–215. [CrossRef]
36. Nagaraju, N.; Surya Prakash, R.; Venkata Ajay Kumar, G.; Ujwala, N.G. Optimization of Electrical Discharge Machining Process Parameters for 17-7 PH Stainless Steel by Using Taguchi Technique. *Mater. Today Proc.* **2020**, *24*, 1541–1551. [CrossRef]
37. Sahoo, R.; Singh, N.K.; Bajpai, V. Approach towards Green Manufacturing in Maglev EDM Using Different Biodegradable Dielectrics at Variable Discharge Conditions. *J. Clean. Prod.* **2023**, *430*, 139623. [CrossRef]
38. Liu, L.; Thangaraj, M.; Karmiris-Obratański, P.; Zhou, Y.; Annamalai, R.; Machnik, R.; Elsheikh, A.; Markopoulos, A.P. Optimization of Wire EDM Process Parameters on Cutting Inconel 718 Alloy with Zinc-Diffused Coating Brass Wire Electrode Using Taguchi-DEAR Technique. *Coatings* **2022**, *12*, 1612. [CrossRef]
39. Ishfaq, K.; Sana, M.; Ashraf, W.M.; Dua, V. Sustainable EDM of Inconel 600 in Cu-Mixed Biodegradable Dielectrics: Modelling and Optimizing the Process by Artificial Neural Network for Supporting Net-Zero from Industry. *J. Clean. Prod.* **2023**, *421*, 138388. [CrossRef]
40. Sharma, V.; Sabiruddin, K. A Comparative Study of Sand-Blasted and Electro-Discharge-Machined Surfaces of Steel Substrates. *Sadhana-Acad. Proc. Eng. Sci.* **2020**, *45*, 50. [CrossRef]
41. Yang, C.; Yin, C.; Wu, Y.; Zhou, Q.; Liu, X. Atomic Insights into the Deformation Mechanism of an Amorphous Wrapped Nanolamellar Heterostructure and Its Effect on Self-Lubrication. *J. Mater. Res. Technol.* **2023**, *26*, 4206–4218. [CrossRef]
42. Jiang, Y.L.; Fang, J.X.; Ma, G.Z.; Tian, H.L.; Zhang, D.B.; Cao, Y. Microstructure and Properties of an As-Deposited and Post Treated High Strength Carbide-Free Bainite Steel Fabricated via Laser Powder Deposition. *Mater. Sci. Eng. A* **2021**, *824*, 141791. [CrossRef]
43. Hu, J.; Yang, K.; Wang, Q.; Zhao, Q.C.; Jiang, Y.H.; Liu, Y.J. Ultra-Long Life Fatigue Behavior of a High-Entropy Alloy. *Int. J. Fatigue* **2023**, *178*, 108013. [CrossRef]
44. Sahu, A.K.; Mahapatra, S.S.; Bhoi, N.K.; Singh, H.; Leite, M.; Goel, S. Experimental Investigation on Microwave Sintered Composite Tool for Electro-Discharge Machining of Titanium Alloy. *J. Mater. Eng. Perform.* **2022**, *31*, 5026–5041. [CrossRef]
45. Selvarajan, L.; Venkataramanan, K. Surface Morphology and Drilled Hole Accuracy of Conductive Ceramic Composites Si_3N_4-TiN and $MoSi_2$-SiC on EDMed Surfaces. *Wear* **2023**, *530–531*, 204973. [CrossRef]
46. Kuang, W.; Wang, H.; Li, X.; Zhang, J.; Zhou, Q.; Zhao, Y. Application of the Thermodynamic Extremal Principle to Diffusion-Controlled Phase Transformations in Fe-CX Alloys: Modeling and Applications. *Acta Mater.* **2018**, *159*, 16–30. [CrossRef]
47. Papazoglou, E.L.; Karmiris-Obratański, P.; Leszczyńska-Madej, B.; Markopoulos, A.P. A Study on Electrical Discharge Machining of Titanium Grade2 with Experimental and Theoretical Analysis. *Sci. Rep.* **2021**, *11*, 8971. [CrossRef]
48. Taguchi, G.; Chowdhury, S.; Wu, Y. *Taguchi's Quality Engineering Handbook*; Taylor & Francis: Boca Raton, FL, USA, 2007.

49. Kechagias, J.D.; Zaoutsos, S.P. Optimising Fused Filament Fabrication Surface Roughness for a Dental Implant. *Mater. Manuf. Process.* **2023**, *38*, 954–959. [CrossRef]

50. Ilani, M.A.; Khoshnevisan, M. Powder Mixed-Electrical Discharge Machining (EDM) with the Electrode Is Made by Fused Deposition Modeling (FDM) at Ti-6Al-4V Machining Procedure. *Multiscale Multidiscip. Model. Exp. Des.* **2020**, *3*, 173–186. [CrossRef]

51. Bhiradi, I.; Hiremath, S.S. Energy Efficient and Cost Effective Method for Generation of In-Situ Silver Nanofluids: Formation, Morphology and Thermal Properties. *Adv. Powder Technol.* **2020**, *31*, 4031–4044. [CrossRef]

52. Zhou, C.; Ren, Z.; Lin, Y.; Huang, Z.; Shi, L.; Yang, Y.; Mo, J. Hysteresis Dynamic Model of Metal Rubber Based on Higher-Order Nonlinear Friction (HNF). *Mech. Syst. Signal Process.* **2023**, *189*, 110117. [CrossRef]

53. Zeng, L.; Lv, T.; Chen, H.; Ma, T.; Fang, Z.; Shi, J. Flow Accelerated Corrosion of X65 Steel Gradual Contraction Pipe in High CO_2 Partial Pressure Environments. *Arab. J. Chem.* **2023**, *16*, 104935. [CrossRef]

54. Yang, Z.; Tang, B.; Qiu, Y.; Wu, J.; Wei, W.; Huang, X.; Luo, X.; Wu, G. Measurement of Transient Temperature Using Laser-Induced Breakdown Spectroscopy (LIBS) with the Surface Temperature Effect. *J. Anal. At. Spectrom.* **2023**, *38*, 1952–1961. [CrossRef]

55. Niamat, M.; Sarfraz, S.; Ahmad, W.; Shehab, E.; Salonitis, K. Parametric Modelling and Multi-Objective Optimization of Electro Discharge Machining Process Parameters for Sustainable Production. *Energies* **2020**, *13*, 38. [CrossRef]

56. Yavari, S.; Modabberifar, M.; Sheykholeslami, M.R. An Experimental Investigation of Electro Discharge Machining Parameters Effects on Ferromagnetic Properties of Extra-Low-Carbon Steel. *J. Magn. Magn. Mater.* **2022**, *549*, 169041. [CrossRef]

57. Wasif, M.; Khan, Y.A.; Zulqarnain, A.; Iqbal, S.A. Analysis and Optimization of Wire Electro-Discharge Machining Process Parameters for the Efficient Cutting of Aluminum 5454 Alloy. *Alex. Eng. J.* **2022**, *61*, 6191–6203. [CrossRef]

58. Jahare, M.H.; Idris, M.H.; Hassim, M.H. Effect of WEDM Parameters on Material Removal Rate and Kerf's Width of Cobalt Chromium Molybdenum Using Full Factorials Design. *Adv. Mater. Process. Technol.* **2022**, *8*, 550–563. [CrossRef]

59. Mushtaq, R.T.; Iqbal, A.; Wang, Y.; Khan, A.M.; Abu Bakar, M.S. Parametric Optimization of 3D Printing Process Hybridized with Laser-Polished PETG Polymer. *Polym. Test.* **2023**, *125*, 108129. [CrossRef]

60. Mushtaq, R.T.; Wang, Y.; Rehman, M.; Khan, A.M.; Bao, C.; Sharma, S.; Eldin, S.M.; Abbas, M. Investigation of the Mechanical Properties, Surface Quality, and Energy Efficiency of a Fused Filament Fabrication for PA6. *Rev. Adv. Mater.* **2023**, *62*, 20220332. [CrossRef]

61. Bhiradi, I.; Raju, L.; Hiremath, S.S. Adaptive Neuro-Fuzzy Inference System (ANFIS): Modelling, Analysis, and Optimisation of Process Parameters in the Micro-EDM Process. *Adv. Mater. Process. Technol.* **2020**, *6*, 133–145. [CrossRef]

62. Cakiroglu, R. Analysis of EDM Machining Parameters for Keyway on Ti-6Al-4V Alloy and Modelling by Artificial Neural Network and Regression Analysis Methods. *Sadhana-Acad. Proc. Eng. Sci.* **2022**, *47*, 150. [CrossRef]

63. Priyadarshini, M.; Vishwanatha, H.M.; Biswas, C.K.; Singhal, P.; Buddhi, D.; Behera, A. Effect of Grey Relational Optimization of Process Parameters on Surface and Tribological Characteristics of Annealed AISI P20 Tool Steel Machined Using Wire EDM. *Int. J. Interact. Des. Manuf.—IJIDEM* **2022**, 1–10. [CrossRef]

64. Singh, R.; Hussain, S.A.I.; Dash, A.; Rai, R.N. Modelling and Optimizing Performance Parameters in the Wire-Electro Discharge Machining of Al5083/B_4C Composite by Multi-Objective Response Surface Methodology. *J. Braz. Soc. Mech. Sci. Eng.* **2020**, *42*, 344. [CrossRef]

65. Majumdar, S.; Bhoi, N.K.; Singh, H. Graphene Nano-Powder Mixed Electric Discharge Machining of Inconel 625 Alloy: Optimization of Process Parameters for Material Removal Rate. *Int. J. Interact. Des. Manuf.—IJIDEM* **2022**, *17*, 2341–2347. [CrossRef]

66. Bose, S.; Nandi, T. Measurement of Performance Parameters and Improvement in Optimized Solution of WEDM on a Novel Titanium Hybrid Composite. *Measurement* **2021**, *171*, 108811. [CrossRef]

67. Sivaiah, P.; Chakradhar, D. Modeling and Optimization of Sustainable Manufacturing Process in Machining of 17-4 PH Stainless Steel. *Measurement* **2019**, *134*, 142–152. [CrossRef]

68. Lau, W.S.; Wang, M.; Lee, W.B. Electrical Discharge Machining of Carbon Fibre Composite Materials. *Int. J. Mach. Tools Manuf.* **1990**, *30*, 297–308. [CrossRef]

69. Gourgouletis, K.; Vaxevanidis, N.M.; Galanis, N.I.; Manolakos, D.E. Electrical Discharge Drilling of Carbon Fibre Reinforced Composite Materials. *Int. J. Mach. Mach. Mater.* **2011**, *10*, 187–201. [CrossRef]

70. Habib, S.; Okada, A. Study on the Movement of Wire Electrode during Fine Wire Electrical Discharge Machining Process. *J. Mater. Process. Technol.* **2016**, *227*, 147–152. [CrossRef]

71. Lodhi, B.K.; Verma, D.; Shukla, R. Optimization of Machining Parameters in EDM of CFRP Composite Using Taguchi Technique. *Int. J. Mech. Eng. Technol.* **2014**, *5*, 70–77.

72. Maegawa, S.; Morikawa, Y.; Hayakawa, S.; Itoigawa, F.; Nakamura, T. A Novel Cutting Concept of CFRP Composites for Extending the Life of Tool. *Key Eng. Mater.* **2015**, *656–657*, 198–203. [CrossRef]

73. Sheikh-Ahmad, J.Y. Hole Quality and Damage in Drilling Carbon/Epoxy Composites by Electrical Discharge Machining. *Mater. Manuf. Process.* **2016**, *31*, 941–950. [CrossRef]

74. Sheikh-Ahmad, J.Y.; Shinde, S.R. Machinability of Carbon/Epoxy Composites by Electrical Discharge Machining. *Int. J. Mach. Mach. Mater.* **2016**, *18*, 3–17. [CrossRef]

75. Teicher, U.; Müller, S.; Münzner, J.; Nestler, A. Micro-EDM of Carbon Fibre-Reinforced Plastics. *Procedia Cirp* **2013**, *6*, 320–325. [CrossRef]

76. Kumar, R.; Agrawal, P.K.; Singh, I. Fabrication of Micro Holes in CFRP Laminates Using EDM. *J. Manuf. Process.* **2018**, *31*, 859–866. [CrossRef]

77. Hassan, A.; He, Y.L.; Rehman, M.; Ishfaq, K.; Zahoor, S.; Hussain, M.Z.; Siddique, F.; Wang, D.C. Machinability Investigation in Electric Discharge Machining of Carbon Fiber Reinforced Composites for Aerospace applications. *Polym. Compos.* **2022**, *43*, 7773–7788. [CrossRef]

78. Farooq, M.U.; Anwar, S.; Ali, M.A.; Hassan, A.; Mushtaq, R.T. Exploring Wide-Parametric Range for Tool Electrode Selection Based on Surface Characterization and Machining Rate Employing Powder-Mixed Electric Discharge Machining Process for Ti6Al4V ELI. *Int. J. Adv. Manuf. Technol.* **2023**, *129*, 2823–2841. [CrossRef]

79. Park, S.; Kim, G.; Lee, W.; Min, B.-K.; Lee, S.-W.; Kim, T.-G. Microhole machining on precision cfrp components using electrical discharging machining. In Proceedings of the 20th International Conference on Composite Materials (ICCM 2015), Copenhagen, Denmark, 19–24 July 2015.

80. Mushtaq, R.T.; Iqbal, A.; Wang, Y.; Cheok, Q.; Abbas, S. Parametric Effects of Fused Filament Fabrication Approach on Surface Roughness of Acrylonitrile Butadiene Styrene and Nylon-6 Polymer. *Materials* **2022**, *15*, 5206. [CrossRef]

81. Wu, D.Z.; Wei, Y.P.; Terpenny, J. Predictive Modelling of Surface Roughness in Fused Deposition Modelling Using Data Fusion. *Int. J. Prod. Res.* **2019**, *57*, 3992–4006. [CrossRef]

82. Mushtaq, R.T.; Iqbal, A.; Wang, Y.; Khan, A.M.; Petra, M.I. Advancing PLA 3D Printing with Laser Polishing: Improving Mechanical Strength, Sustainability, and Surface Quality. *Crystals* **2023**, *13*, 626. [CrossRef]

83. Mushtaq, R.T.; Wang, Y.; Khan, A.M.; Rehman, M.; Li, X.; Sharma, S. A Post-Processing Laser Polishing Method to Improve Process Performance of 3D Printed New Industrial Nylon-6 Polymer. *J. Manuf. Process.* **2023**, *101*, 546–560. [CrossRef]

84. Khan, M.S.; Mishra, S.B. Minimizing Surface Roughness of ABS-FDM Build Parts: An Experimental Approach. *Mater. Today Proc.* **2019**, *26*, 1557–1566. [CrossRef]

85. Mohamed, O.A.; Masood, S.H.; Bhowmik, J.L. Experimental Investigation for Dynamic Stiffness and Dimensional Accuracy of FDM Manufactured Part Using IV-Optimal Response Surface Design. *Rapid Prototyp. J.* **2017**, *23*, 736–749. [CrossRef]